Scientia Horticulturae 209 (2016) 1–13

Contents lists available at ScienceDirect

Scientia Horticulturae

journal homepage: www.elsevier.com/locate/scihorti

Use of digital images to disclose canopy architecture in olive tree

M. Moriondo[a,*], L. Leolini[b], N. Staglianò[b], G. Argenti[b], G. Trombi[b], L. Brilli[b], C. Dibari[b], C. Leolini[c], M. Bindi[b]

[a] CNR-IBIMET, Via G. Caproni 8, 50145, Florence, Italy
[b] Department of Agri-Food Production and Environmental Sciences (DiSPAA), University of Florence, P.le delle Cascine 18, 50144, Florence, Italy
[c] Student of School of Mechanical Engineering, University of Florence, Via S. Marta 3, 50139, Florence, Italy

ARTICLE INFO

Article history:
Received 17 March 2016
Received in revised form 10 May 2016
Accepted 25 May 2016
Available online 17 June 2016

Keywords:
Canopy architecture
3D modelling
Point cloud
Random forest
Phenotyping platform

ABSTRACT

The use of digital cameras for monitoring natural vegetation and agricultural ecosystems is particularly attractive since it necessitates neither expensive equipment nor extensive skill. In this study we tested the use of digital images (DIs) to generate 3D plant reconstruction for retrieving the main plant architectural features (leaf area, leaf inclination, leaf azimuth) of olive tree branches. High resolution image of tree branches were firstly used to generate 3D reconstruction of plant structures using a Structure From Motion approach; we therefore answered the question whether these 3D models may be segmented to discriminate main plant structures (leaves and branch) proposing a simple classification algorithm (Random Forest, RF) with saliency features and color indices as predictors. Finally, on the good and robust performances of the proposed classification algorithm, the single leaves were analyzed to retrieve the relevant area, inclination and orientation and compared to the relevant observed data. The calibration of the RF model indicated that color indices better discriminated leaves and stem than the sole use of saliency features. The classification performances were further improved by tuning the scale at which saliency features were calculated and by filtering the final result to reduce misclassified points. A RF model calibrated on a single plant was successfully applied to 5 others, indicating the robustness of the calibration strategy. The analysis of single leaves, as segmented after the classification process, indicated that plant architecture was satisfactorily reproduced with strong correlations obtained between measured and calculated values of leaf inclination and azimuth, while biases were observed for leaf area. These results emphasize the effectiveness of SFM in reproducing complex arrangements of leaves like on an olive tree. The use of such a system can be therefore suggested as a first step towards an improved low cost plant phenotyping platform to speed up our understanding of plant responses to environment. Further experiments are required to test the effectiveness of the approach also under outdoor conditions.

1. Introduction

An accurate estimate of plant architecture is of major importance for the ecological characterization of a natural or agricultural ecosystem, and digital images (DIs) have often been exploited for this purpose since the approach is not destructive, not time consuming and necessitates neither expensive equipment nor extensive skill (Li et al., 2014).

Many applications address the measurement of leaf area spatial distribution (Leaf Area Index, LAI), since this parameter plays a major role as plant interface with the atmosphere and determines biomass accumulation (Liu et al., 2013a; Macfarlane et al., 2007; Fuentes et al., 2008; Chianucci et al., 2014). The use of DIs is centered on the indirect estimation of canopy structural variables such as gap fraction (GF) or its complement (foliage cover, FC), clumping index (CI) and leaf inclination angles (LIA) (Ryu et al., 2010; Pisek et al., 2011; Liu et al., 2013b; Zou et al., 2014), which are then combined for LAI estimation according to the Beer-Lambert's law (Brantley and Young, 2007) The approaches generally used for the estimation of these indexes are based on single DIs taken by commercial cameras above or below the canopy depending on the ecosystem under analysis, the parameter to be estimated or the specific approach developed. E.g. for forest ecosystems Fuentes et al. (2008) estimated GF using horizontal upward-facing DIs, whereas Chianucci et al. (2014) obtained the same information using downward-facing DIs taken from above the canopy, while LIA was estimated using a digital leveled camera at several heights in the canopy. In agro-ecosystems, GF estimated using DIs acquired below the canopy have been proven to provide results for LAI estimation compara-

* Corresponding author.
E-mail addresses: marco.moriondo@cnr.it (M. Moriondo), marco.moriondo@cnr.it (M. Bindi).

http://dx.doi.org/10.1016/j.scienta.2016.05.021
0304-4238/

ble to those obtained with commercial instruments (Confalonieri et al., 2013).

In a more comprehensive approach, DIs were taken orthogonally around a tree in the main directions, and GF analysis used for reconstructing tree crown volume and vertical profile of leaf area of isolated trees (Phattaralerphong and Sinoquet, 2005; Phattaralerphong et al., 2006). In other words, this system provides the basis to capture the third dimension (3D) in plant geometry that enables height and volumetric analysis, which cannot otherwise be calculated using traditional approaches.

The rapid technological development in DI-based photogrammetry made new tools and algorithms available for researchers that allow the 3D features of a scene to be obtained. Ivanov et al. (1995) proposed the first approach using stereo vision (SV) to reconstruct the 3D surface of a cultivar for measurement and analysis and this represents another step towards the fine quantification of plant geometry at spatial and temporal resolutions that are not easily achieved with a 2D image analysis. The SV system, often composed of two cameras aligned in a fixed structure, relies on the detection of corresponding points in the acquired stereo images. The analysis of relative positions of these points traced in the images provides the depth information (disparity) of the respective pixels. The resulting disparity map is then converted into a point cloud xyz with a given system of coordinates, which may be further classified and segmented to analyze plant structures. The framework described in Müller-Linow et al. (2015) provides evidence on the effectiveness of this approach in the estimation of LAI and LIA of herbaceous plant populations and single trees both in the laboratory and under field conditions.

Jay et al. (2015) pointed out that the structure from motion (SFM) approach, which simultaneously estimates the camera position and the structure and position of objects in the scene, is an alternative approach to retrieve a point cloud from DIs, which does not necessitate either expensive equipment or extensive skill. In practical terms, SFM solves the same problem as SV (i.e. seeking matching points from images and reconstruction of a 3D object), by processing a set of overlapping photographs of an object to create a 3D point cloud that represents the structure of the objects under analysis.

While SFM-based 3D models have been used extensively to reproduce urban features (Snavely et al., 2008; Pollefeys et al., 2004), natural vegetation (Dandois and Ellis, 2010; Turner et al., 2011) or agricultural areas (Mathews and Jensen, 2013; Zarco-Tejada et al., 2014; Díaz-Varela et al., 2015), their potential application in plant architectural analysis has still to be explored (Jay et al., 2015).

On these premises, in this study we tested the use of DIs as the core of a simplified phenotyping platform, which relies on the use of a SFM approach for retrieving the main plant architectural features (leaf area, leaf inclination, leaf azimuth) of olive tree branches. This test considers four basic steps: (i) high resolution image acquisition of olive tree branches under indoor conditions and generation of relevant point clouds via SFM; (ii) calibration of a classification algorithm (Random Forest, RF) to discriminate leaves and branch structures using saliency features (i.e. descriptors of shape) and color indices; (iii) segmentation of leaves and iv) analysis of single leaves to retrieve the relevant area, inclination and orientation. These steps are described and discussed separately.

2. Material and methods

2.1. Image acquisition

High-resolution TIFF images of a single branch of 6 potted 4-year old olive trees (*Olea europaea* L., var. *Frantoio*) were acquired in the laboratory in 2015 on 6 different plants, on days of year (DOY) 28, 37, 65, 79, 90, 118, 125, under natural indoor diffused radiation and used to reconstruct the relevant plant structures using an SFM approach (Table 1). A north-oriented vertical leveled panel with a grid of markers was placed behind the plant to mask surrounding objects and provide a grid for re-scaling the point clouds to a common reference system (Fig. 1 step 1).

Table 1
Description of branch under analysis. Legend: DOY = day of year of analysis, PStage = phenological stage (D = dormancy, SE = shoot elongation); TLN total leaf number on the branch; SL = sampled leaves; NOP = number of pictures taken for each branch. In plant 3 analysis were performed on both a subsample and total leaf number (indicated between brackets). In plant 4 analysis were performed only on the total leaf number.

Plant	DOY	PStage	TLN	NOP	SL
1	37	D	95	120	21
2	65	D	110	125	18
3	79	D	116	130	24 (116)
4	90	D	135	150	135
5	118	SE	140	150	39
6	125	SE	160	180	39

The number of DIs acquired was chosen bearing in mind that for a good 3D reconstruction the degree of overlap between two adjacent images should be at least 70% (James and Robson, 2012). In our specific case, the images were captured at a high resolution (5202 × 3465 pixels) using a leveled digital camera (CANON EOS D600) mounted on a tripod placed at as average distance of 0.5 m from the plant, which was moved spanning along the vertical and horizontal profiles of each branch. The final number of DIs depended on the dimension of the scene and the field of view (FOV) of the camera: considering as an example, an average focal length of 30 mm and a distance to subject of 0.5 m, the picture would have a horizontal FOV 37 cm and a vertical FOV of 25 cm. Considering an overlapping degree of 80% between pictures on both horizontal and vertical directions, this would result into pictures taken on a step of 7.5 cm and 5 cm respectively. When applied to a scene of e.g. 70 × 70 cm, this results into ∼10 pictures spanning the horizontal axis and 14 spanning the vertical one for a total of 140 pictures.

Given that SFM approach for 3D reconstruction relies on the identifications of points that are seen on several images, there is the need to keep in focus the objects of interest in the scene otherwise much information on the texture would be lost and the identification of points would be difficult. Accordingly, we increased the depth of field of the camera by reducing the aperture of the lens diaphragm (f. 22).

After the acquisition of DIs, azimuth, inclination and area of each leaf were measured. A digital compass installed on Apple IPhone 5 S® was used to measure leaf azimuth, which was computed clockwise as the angle between north and the horizontal projection of the vector lying on the leaf middle rib and centered on the leaf insertion. Leaf inclination was determined on DIs acquired by a leveled smartphone-camera application (LVL CAM) for each single leaf according to Pisek et al. (2011). In this case, the leveled camera was moved around each leaf manually until the leaf was found to be normally oriented to the camera's viewing direction. These operations (azimuth measures and acquisition of leaf images) were performed at a safe distance taking care not disturbing the original position of plant structures.

After azimuth measurement and acquisition of leveled DI of leaves on the plant, each leaf was removed, placed on a white background and photographed orthogonally from above for leaf area calculation (see next section).

On each sampling DOY, point clouds of plant were reconstructed, labelled leaves were identified on screen and the relevant inclination, azimuth and leaf area compared to measured values.

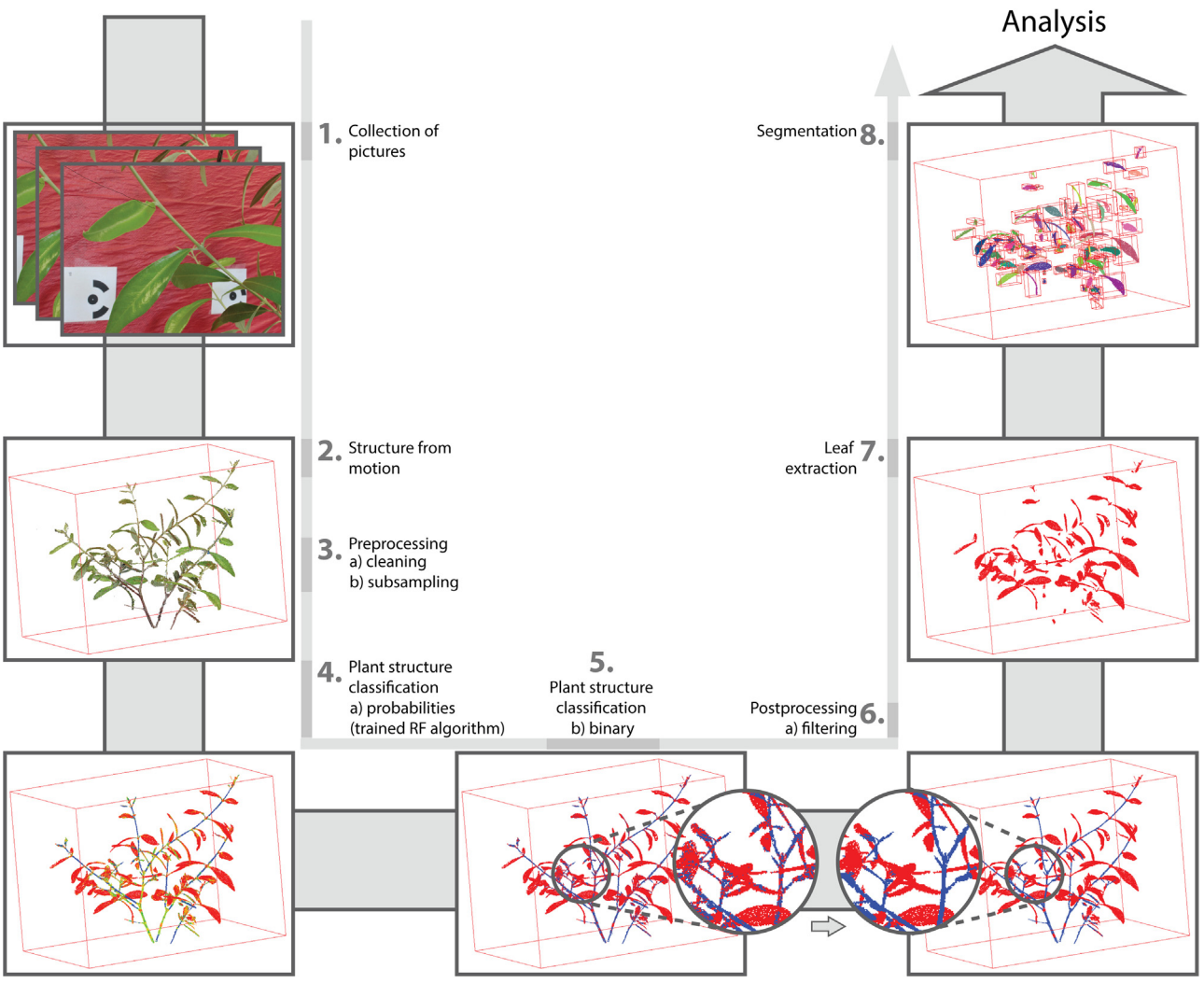

Fig. 1. Procedure for recovering plant structure and leaf segmentation and analysis. Digital images were used to provide a 3D reconstruction of an olive branch (steps 1–2) that after cleaning and subsampling (step 3), was classified according to a calibrated machine learning algorithm into its main structures (leaves and stem) (steps 4–5). After filtering (step 6), leaves were segmented and then analyzed to derive the relevant area, inclination and azimuth (steps 7–8).

On DOY 65 and 79, the features of the entire leaf population were measured and estimated, and the relevant distributions compared.

2.2. Image processing

DIs of plants 1–6 were firstly processed using Matlab (ver. R2007b) to remove the red background using RGB digital numbers (DNs), which were combined according to Eq. (1) to derive a grayscale image enhancing the difference between the panel in the background and the olive tree branch.

$$S = (R + G + B) / (2 \times R - G) \quad (1)$$

where S is the output gray level of the image and R = red DN, G = green DN B = blue DN on the input image.

The image contrast (H) was then increased by stretching its original values. A median filter using a 20 by 20 pixels window was then applied to the resulting image to reduce the noise effect (i.e. each output pixel contains the average value in a 20 by 20 neighborhood around the original pixel). Finally the grayscale image was converted into a binary image changing all pixels in the input image with luminance greater than 0.5 with the value 1 (corresponding to both leaves and stem) and replacing all other pixels (i.e. the background) with value 0.

Leveled DIs of single leaves taken using LVL CAM were processed using ImageJ software (http://rsbweb.nih.gov/ij/) to calculate the angle between the zenith and leaf normal surface (Pisek et al., 2011).

Leaf area of each single leaf was calculated using ImageJ by thresholding the white background on which the images of the removed leaves were acquired.

2.3. Point cloud pre-processing

The 3D olive tree point cloud was obtained using Agisoft PhotoScan ® (Agisoft LLC) in a manually driven operation. The first stage consists in loading photos in the software and in their alignment. In this phase the software searches for a set of common points identified in several pictures taken from different angles that are used to reconstruct the orientation and position of the camera each picture was taken from. The number of key points detected on an image is strictly dependent image texture and resolution and therefore requires complex images at the original resolution as obtained in this experiment (Section 2.). To speed up this process, the masks obtained as described in Section 2.2 were used to constrain the object under analysis (i.e. the olive tree) while removing the background

The estimated camera positions and DIs themselves are further used to retrieve the positions of non-feature point pixels that are finally combined into a single dense point cloud. At this stage, a preliminary filtering operation was automatically performed for filtering points potentially misplaced duo to poor texture of some elements or badly focused images.

Both camera alignment and dense point cloud reconstruction are time-consuming process and the user is then allowed to select a lower or intermediate quality model. However, for this experiment, the highest quality parameters were selected in Photoscan, in order to obtain a detailed 3D model of each plant to be used for classification.

The final 3D reconstructions were rescaled using as a reference system the markers that were placed in the background of each picture (Fig. 1 step 2). The final output of this procedure consisted into a dense point cloud where each point, featured by its xyz coordinates, was associated to the relevant RGB DNs as extracted from the DIs. This object was used for the estimation of plant architecture.

Since 3D models of each branch resulted noisy (i.e. some points were misplaced in the space) and points were not homogeneously distributed (surface point density was variable), obtained point clouds were processed to reduce these issues with a potential impact on classification performances. Point clouds were imported into CloudCompare (v.2.6.0 3D) (Daniel Girardeau-Montaut, 2011), which has tools for removing outliers using a statistical approach, and a subsampling procedure that, while reducing the points to be processed, leads to equally spaced points. The cleaning procedure considers the distribution of average distance of each point from all its neighbors. Assuming a Gaussian distribution of these distances, all points with mean distances outside the range indicated by the global distances mean and the relevant standard deviation are considered as misplaced and removed from the point cloud (Fig. 1 step 3). The number of points for mean distance estimation and the standard deviation were empirically set to find a compromise between the goodness of final output and loss of information due to point reduction. In our experience, given that the standard conditions where the DIs were acquired leaded to 3D models having approximately the same quality, number of points for mean distance estimation and the standard deviation converged to 50 and 0.6 for all the datasets.

After cleaning, each point cloud was subsampled to maintain a minimum distance between points of 0.6 mm.

2.4. Classification

In this study, we trained a machine-learning algorithm (Random Forest, RF) for classification of plant structures that uses both colors and shape information derived from the point cloud as predictor variables (Fig. 1 step 4).

2.4.1. RF classification algorithm

RF (Breiman, 2001) is a classifier consisting of an ensemble of de-correlated decision trees that use as input different bootstrap samples from a randomized subset of the predictor variables. At each iteration, the bootstrap sample is randomly split for training (66%) and internal testing (33%, out-of-bag sample, OOB). A classification tree is grown to each bootstrap sample where for each node the best split is calculated considering only a given number of predictor variables (parameter *mtry*) randomly selected. Each tree is grown up to a final node and it is then used to calculate the error on OOB and this procedure is iterated for a specified number of trees (parameter *ntree*). This strategy provides very well-supported and robust predictions compared with other classifiers (Cutler et al., 2007). Each of classification tree, grown according this procedure, contributes to the model prediction with one vote, where the final model prediction consists of prediction that gets more votes.

Mtry parameter was set rounding up to the square root of the number of 6 input variables (*mtry* = 3).

A preliminary analysis on the performances of RF in the training test demonstrated that the overall classification error no longer decreased for *ntree* >300, which was therefore selected as *ntree* value for plant structures classification.

In RF algorithm the relative importance of each predictor variable in the classification process may be assessed as well as the marginal effect of an individual predictor variable on the class probability. This provides more insight into the effectiveness of the proposed strategy by testing the assumptions made on saliency features (see next section).

2.4.2. Predictor variables

Shape information was retrieved according to the Lalonde et al. (2006) modified for canopy classification. This approach relies on the decomposition into principal component analysis (PCA) of the covariance matrix of the 3D position of n neighboring points. The resulting three ordered eigenvalues (i.e. $\lambda_0 \geq \lambda_1 \geq \lambda_2$) provide information on the spatial distribution of the subset being analyzed: in the case of scattered points (i.e. with no predominant direction) we expect $\lambda_0 \simeq \lambda_1 \simeq \lambda_2$, while for points distributed mainly along one axis we expect $\lambda_0 \geq \lambda_1 \simeq \lambda_2$, which corresponds to a linear structure. Finally, for roughly planar distribution we expect $\lambda_0 \simeq \lambda_1 \geq \lambda_2$. Accordingly, the shape of n neighboring points around a given point x may be summarized using the relevant saliency features λ_0 (named scatter-ness, SC-N), $\lambda_0 - \lambda_1$ (linearness, LI-N) and $\lambda_1 - \lambda_2$ (surface-ness, SU-N). For each point in the point cloud, SC-N, LI-N and SU-N were calculated in the R environment (R-project) considering a different spatial scale (see next section).

RGB data associated to each point in the cloud were used for calculating color indices to provide additional predictor variables for structure classification. The green, red and blue DNs of each point were used to compute the percentage of relative brightness of each channel (GI = green index, RI = red index and BI = blue index) according to Eqs. (2)–(4)

$$GI = G/(R + G + B) \quad (2)$$

$$RI = R/(R + G + B) \quad (3)$$

$$BI = B/(R + G + B) \quad (4)$$

2.4.3. RF calibration and validation strategy

Point cloud data obtained in the 3D reconstruction of an olive tree on DOY 28 were first pre-processed to reduce noisy points and obtain a more regular point density over the space (Section 2.3). This branch was then used for calibrating and validating the classification approach. The relevant point cloud consisted of about 52,000 points that were manually labelled into two classes, stem (17,000 points) and leaves (35,000 points) and divided in two subsets to be used for training and validating the RF classification. Since RF trained with unbalanced data would result into an overestimation of the majority class (Evans et al., 2011), the same number of xyz points was selected for each class in the calibration subset (12,000 points), while the remaining data were used for validation (23,000 for leaves and 5000 for stem).

The resulting datasets were then used for computing saliency features and color indices to be used as predictor variables of RF for recovering the main plant structures (leaves and stem).

In this process, these variables were initially independently used for calibrating RF to highlight the relative importance of saliency features (SC-N, LI-N and SU-N) and color indices (RI, GI, BI) as predictor variables and the relative performances were compared in terms of goodness of fit. A single RF was then calibrated using both saliency features and color indices as predictor variables.

To boost the computational efficiency in the calculation of saliency features, point cloud data were organized in a KD-tree for a faster retrieval of local neighboring points around each point. In other words, for each point in the cloud, KD-tree identifies the *n* nearest neighbor points to be used in the saliency features calculation.

Considering that the classification performances may be strongly affected by the scale at which the saliency features are calculated (i.e. the number of nearest neighbor points), RF was trained using different KD-tree structures, ranging from 30 to 600 points, and the relative performances in the validation subset were compared. Accordingly, the RF model was calibrated and validated considering datasets where saliency features were computed for an increasing number of nearest points to each point in the cloud. The relative effect of each scale in determining the final performance of the model was compared in terms of goodness of fit.

2.4.4. Filtering

A pointwise filtering approach was introduced to reduce the impact of classification error on the overall classification performances (Fig. 1 step 5). For each point initially classified as stem (linear), a filter was applied to compute the most frequent class above a threshold present in the neighborhood and to change the original point class to this value. A second filter with similar characteristics was then applied to points initially classified as surface. Since it is unclear what the minimum number of points (or the range) to be processed should be or the threshold above which the class of a point should be converted into the other, these parameters were calibrated using the classified point cloud from the validation dataset. This dataset was previously organized in KD-trees with increasing complexity, from 30 to 600 points (step 20). For each KD-tree, the algorithm computes the relative presence of points belonging to stem and leaves for each point initially classified as linear. As second step, the filter is applied on points initially classified as area using the same procedure. The class of each point is then converted to the new class only when the ratio of neighboring points belonging to the new class exceeds a certain threshold between 0.1 and 1.

2.5. Segmentation

A label connected components algorithm (CCA), as implemented in CloudCompare was applied to the points classified as leaves to decompose them into sub-clouds, each of which represented a single leaf (Fig. 1 step 8). The algorithm, originally developed for images (e.g. Yang and Zhang, 2003), was extended to point clouds analysis, where the user is allowed to set the minimum number of points that are part of a component and the minimum gap between two components. In this experiment, we selected 100 as the minimum number of points (corresponding to a surface of $\sim$54 mm^2) and a threshold distance of 0.9 mm between elements (given the fact that the points are equally spaced 0.6 $\times$ 0.6 mm).

2.6. Leaf inclination, azimuth and area calculation

After segmentation, each leaf was separately analyzed using Matlab 7.0a (Mathworks Inc.) to extract the relevant inclination, azimuth and area (Fig. 1 step 9).

For each point cloud classified as leaf, a single polygon containing all xyz points of the segmented leaf was created using a convex hull approach and the relevant polygon area was calculated. This simplified approach was preferred to the leaf area calculated using a meshed point cloud due to potential impact of a noisy classification of leaf surface.

A plane was fitted to the n xyz points representing a leaf to calculate leaf inclination. The vector normal to that plane centered on the leaf centroid was then obtained and inclination was calculated as the angle spanning from the zenith to normal leaf surface (Fig. 2).

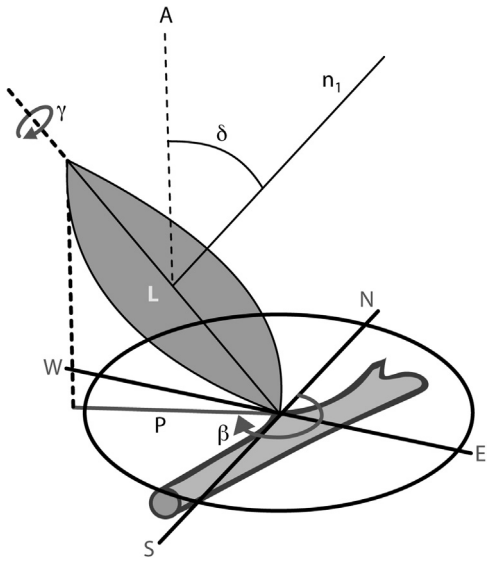

Fig. 2. Leaf angles measurement. Leaf inclination δ, included between the normal to leaf surface n1 and the zenith A, spans between 0 and 90°. The leaf azimuth β, included between north direction N and the projection of leaf middle rib to the plane P, spans between 0° and 360°.

Leaf azimuth was measured clockwise as the angle (°) included between the projection of leaf middle rib on xy-plane and the north direction. The vector describing leaf major axis was oriented along the direction from leaf insertion on the branch to leaf tip (P). Leaf insertion was retrieved considering which of the points more distant from the centroid (i.e. the leaf tips) was closest to the branch.

2.7. Goodness of fit

2.7.1. Classification model

Because the RF model outputs predicted probabilities scaled between 0 (stem) and 1(leaf), a threshold must be selected to transform the scores into a set of stem/leaves predictions. For each RF trained model, each candidate threshold, selected iteratively in the range between 0 and 1 (step 0.1), was applied to the validation dataset to retrieve true positive (a), false positive (b), false negative (c) and true negative (d) cases predicted by the model which were used to produce a corresponding confusion matrix. Model prediction accuracy was then evaluated according to true skill statistic (TSS, Allouche et al., 2006) and the receiver operating characteristic (ROC) curve (Hanley and McNeil, 1982).

TSS is equal to ratio of correct predictions (i.e. sensitivity = a/[a + c]) plus the proportion of correctly predicted absences (i.e. specificity = d/[b + d]) minus 1 (Eq. (5)). TSS values range from −1 to +1, indicating a performance no better than random and perfect agreement, respectively.

$$TSS = sensitivity + specificity - 1 \quad (5)$$

ROC-curve is a graphical method representing, for a range of thresholds, the relationship between the proportion of false positives (i.e. 1-specificity) and the sensitivity. The area under the ROC-curve (AUC), which ranges between 0.5 = worthless test to 1 = perfect test, measures the accuracy of the model to correctly classify the presence or the absence of a given plant structure.

Neither method (TSS or ROC-curve) is affected by prevalence (i.e. unbalanced occurrences amongst classes), but while ROC-curve provides a measure of model performances which are independent from threshold, TSS explicitly indicates the threshold maximizing

prediction accuracy. For each trained RF model, ROC AUC was therefore used to evaluate the quality of the prediction, while the optimal threshold to convert each score to a point belonging to a leaf or a stem was evaluated using TSS.

2.7.2. Leaves features assessment

For each plant, the quality of estimated leaf inclination, azimuth and area was evaluated on both a subsample and on the entire leaf population.

When the comparison was performed on a subsample (i.e. branches of plants 1, 2, 3, 5, 6), each leaf feature was compared to the same unit coming from reconstruction using a regression analysis between true and estimated values. In this case we estimated the goodness of fit according the correlation coefficient R, the root mean square error and mean absolute error (RMSE and MAE). We also analyzed whether the slope of the regression line was significantly different from 1 and if intercept of the same line was significantly different from 0, in order to assess if the regression line was significantly different from the bisector of the xy system of coordinates (i.e. line x = y) that represents the perfect agreement between true and estimated values.

To compare the features of two populations of leaves, i.e. those obtained by sampling leaves from the whole branch (true value) and those obtained after the image reconstruction (estimated value) (branches 3, 4), we applied the non-parametric Kolgromov-Smirnov (KS) test to detect whether the two distributions of leaves for a specific parameter belonged to the same population or not.

3. Results

3.1. RF classification results

The accuracy of the RF model in predicting plant structures (i.e. stem and leaves) was evaluated against the hand-labelled data, considering different KD-tree dimensions.

The calibration of the model indicated that the KD-tree structure is of major importance in determining the performances in the classification process and that color features greatly improved the ability of RF in detecting the structures of olive tree leaves and stem.

As expected, the average maximum radius (MR) from the center of a KD-tree increased in the range between 30 and 600 points, in response to an increasing number of points included in the tree, and this occurred at a different rate for stem and leaves (Fig. 3a) as an effect of their different shapes. Stems, which have a prevalently linear structure, showed a much more evident increase in MR than leaves, which conversely expand along two principal directions.

In general, both TSS and ROC, calculated for the RF trained using datasets where saliency features were obtained in response to different KD-tree dimensions indicated that the classification performances increase up to threshold, above which the ability of RF in detecting the plant structures clearly decreases (Fig. 3bc). When RF was trained separately for saliency features, TSS and ROC peaked in a range between 100 and 200 points with a maximum TSS = 0.40 and ROC = 0.79. The saliency features were outperformed by the RF trained using color indices as predictor, which yielded a maximum TSS = 0.63 and ROC = 0.84 (of course not dependent on the dimensions of the KD-tree). The joint use of saliency features and color indices further improved the RF performances in the classification of stem and leaves, resulting in a maximum TSS = 0.66 and ROC = 0.89, which corresponded in both cases to a threshold of 120 points in the KD-tree (Fig. 3bc). For this specific model and KD-tree dimension, the optimal threshold maximizing TSS (i.e. the threshold to convert each score into leaf or stem) was 0.65 (i.e. points with

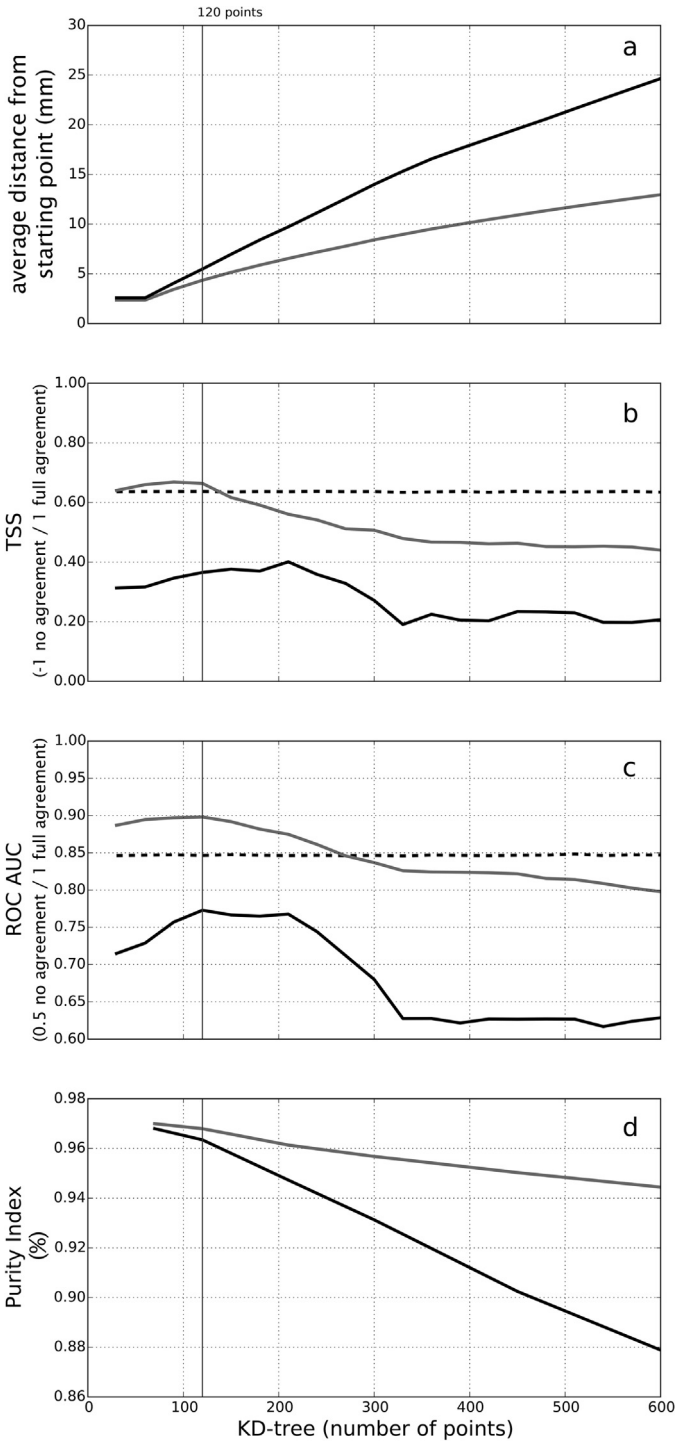

Fig. 3. Structure analysis and classification performances in response to different KD-tree dimensions. (a) Average range of KD-trees (i.e. the average maximum distance from the central point of each KD-tree) in response to their dimensions obtained for stem (black line) and leaves (grey line); (b) and (c) Classification performances (TSS and ROC) of Random Forest in response to different KD-tree dimensions used to calculate saliency features (black line). The dotted lines represent the performances of RF using only color indices as predictors that are insensitive to KD-tree scale. The grey lines show the cumulative performances of RF using both saliency features and color indices as predictors of leaves and stem. (d) Average percentage of points belonging to leaves (grey line) and stem (black line) in KD-trees in response to increasing KD-tree dimensions. The vertical line indicates the KD-tree dimension (120 points) optimizing the classification performances of RF.

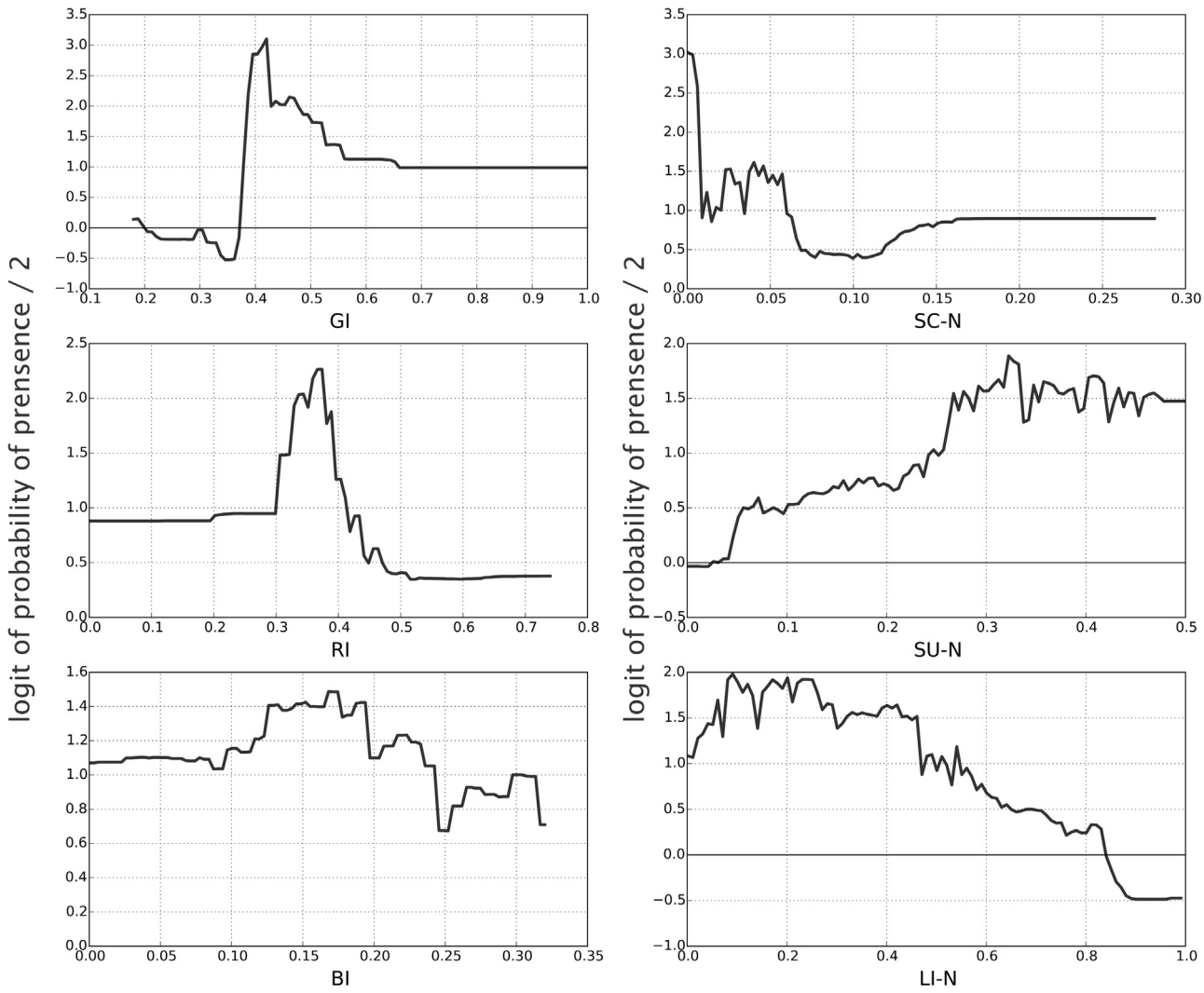

Fig. 4. Partial dependence plots for variables (color indices GI = green index, RI = red index and BI = blue index; saliency features SC-N = scatter-ness, LI-N = linear-ness and SU-N = surface-ness) selected as predictors for olive tree leaves. This represents a measure of the dependence of the probability of presence on one predictor after averaging out the effects of the other predictor variables in the RF model.

a score >0.65 were assigned to a leaf, while those with a score <0.65 to a stem).

Interestingly, the number of points in the KD-tree that maximizes the differences between stem and leaves shapes (i.e. 600) does not correspond to the number of points that maximizes the performances of the final RF model (i.e. saliency features + color indices) (120). In other words, the scale analysis pointed out that increasing distances from the point to be classified results in a noisier classification of olive tree structures. This effect is likely related to the contribution of points that are too far from the point being analyzed, which provides erroneous information about the local shape around the point (e.g. the KD-tree includes an increasing number of points not belonging to the same class, precluding an effective calculation of saliency features). Fig. 3d clearly indicates that the purity of the KD-tree for a particular class (i.e. the percentage of points in the KD-tree belonging to the class of the point being analyzed) declines linearly as the KD-tree dimensions increase.

The analysis of the relative importance of predictor variables in the classification process indicated that GI had the overall greatest impact on the performances of RF, followed by SC-N, LI-N and with RI and SU-N on the same level of importance. BI yielded the lowest importance (Fig. 4).

Inspection of the partial plot indicated that GI and RI have a peak, corresponding to the greatest probability of detecting a point belonging to a leaf, clearly centered on 0.42 and 0.37 of the relevant spectra. By contrast, BI did not present a clear peak in the probability of leaf detection, which ranged from 0.12 to 0.19 of its spectrum.

The partial plot obtained for saliency features confirmed that the probability of detecting a point belonging to a leaf is strictly related to an increased value of SU-N, i.e. to an object with axis oriented along two prevalent directions, and negatively related to increasing LI-N that is more related to linear structures (i.e. stem). SC-N, in the absence of solid objects in the point cloud, is redundant with respect to SU-N, indicating a maximum probability of a point belonging to a leaf close to 0, which corresponds to a maximum difference in $\lambda_1 - \lambda_2$ (Fig. 4).

3.2. Filtering

The overall results indicated that both KD-tree dimensions and threshold play a major role in determining the performances of the filtering: the grid plotting of TSS and ROC in response to these variables identified a range between 100 and 300 for KD-tree dimensions and a threshold of approximately 0.6 as the best combination to optimize the classification of structures, which improved to TSS = 0.78 and a ROC = 0.89 with respect to the TSS = 0.63 and ROC = 0.84 in the original classification (Fig. 5).

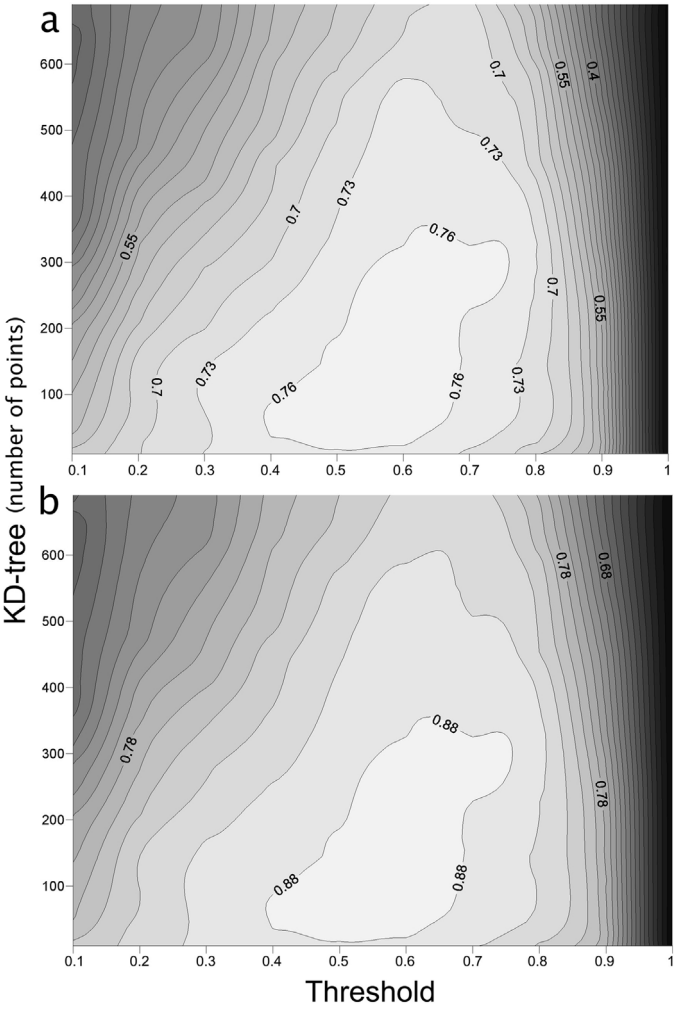

Fig. 5. Classification performances (TSS in (a) ROC AUC in (b) obtained by filtering a classified point cloud using different KD-tree dimensions (y axis) and thresholds to convert one class into another (from stem to leaf).

According to these results, a single RF model, using both color indices and saliency features (for KD-tree = 120) as predictors, was finally trained and used to predict the structure of the olive trees. The results of each classification process were first converted into a point cloud with two classes (leaves and stem) using the threshold maximizing TSS (0.65) and further processed by filtering (KD-tree = 150 with a threshold = 0.6) to reclassify erroneously classified points (scheme in Fig. 1)

3.3. Segmentation

CCA performed reasonably well, provided that leaves were well defined, in terms of point density and delimited area. In some cases, a partial occlusion in the reconstruction of the leaf resulted in over-segmented leaves (i.e. a single leaf fragmented in 2 or more segments). The same happened when the statistical outlier removal thinned too many points belonging to a single leaf, which therefore resulted as over-segmented. In a few cases leaves were overlapping and the CC failed to separate them. Further in some cases RF and the subsequent filtering resulted in misclassified regions on both leaves and stem structures.

In all these cases, we manually edited the point cloud to join the fragmented leaves into single leaves, partitioning those that were jointed into separate leaves and reclassifying misclassified regions to improve the accuracy in the estimation of plant structures.

3.4. Leaf inclination, azimuth and area calculation

Leaves sub-sampled over the 5 plants, manually labelled and identified on screen, were used to assess a biunique correspondence between measured and calculated leaf area azimuth and inclination. The overall results indicated that these latter were well captured using the proposed methodology whereas leaf area was poorly reproduced (Table 2, Fig. 6).

A robust and significant linear correlation exists between observed and measured leaf inclination ($0.94 > R > 0.91$) and azimuth ($0.98 > R > 0.96$), which also present satisfactory low average error indices with $10.5^\circ > RMSE > 5.6^\circ$ and $8.3^\circ > MAE > 4.1^\circ$ for inclination and $30.9^\circ > RMSE > 17.4^\circ$ and $23.6^\circ > MAE > 15.1^\circ$ for azimuth. For both these features, the slope of the linear regression was not significantly different from 1 (except in 2 cases for azimuth) nor was the intercept significantly different from 0 (except in 2 cases for inclination).

Observed and estimated leaf areas were significantly correlated with $0.93 > R^2 > 0.61$, $2.06 > RMSE > 0.51\,cm^2$ and $1.73 > MAE > 0.4\,cm^2$. Slope was significantly lower than 1 in plant 2 and 3 while in all cases the intercept was not significantly different from 0.

KS tests on branches 3 and 4 confirmed the results obtained on the subsamples, indicating that the homogeneity may be accepted for leaf inclination and azimuth ($P > 0.05$), whereas differences exist in estimated and observed leaf area populations (Table 2).

4. Discussion

Several techniques are available nowadays to capture the 3D structure of plants, including LIDAR (Weiss and Biber, 2011), Laser Scanner (Paulus et al., 2013), Kinect Microsoft® (Chéné et al., 2012), stereovision (Müller-Linow et al., 2015), but all these approaches require expensive technical skill to implement and use. Conversely, the application of a typical SFM approach basically requires the use of a digital camera and a software, which is generally available at low cost or even at no cost, such as MicMac (Ign, 2013) or VisualSFM (Wu, 2011), to render point clouds of a scene. These features make the use of SFM particularly attractive for the study of plant structure and architecture using low-cost equipment requiring no special skills. So far only a few studies have considered this possibility. Santos and de Oliveira (2012) concluded that SFM may be successfully applied for plant 3D modelling while Dey et al. (2012) focused their attention on the identification of plant structures in grapevine, not extending their analysis to retrieve plant architectural features. To our knowledge, only Jay et al. (2015), Rose et al. (2015) and Yihang et al. (2014) successfully tested SFM for the retrieval of two main plant structural parameters of a crop (plant height and total/single leaf area). In line with these authors, we tested the effectiveness of a digital camera as core of a simplified phenotyping platform to capture plant structures and architecture at a higher detail (leaf inclination, azimuth and area of each single leaf), using olive trees as test samples. The framework we set up for the purpose considered that the precise reconstruction of plant architecture is strictly related to efficient recognition of the different plant organs captured in the point cloud (Paulus et al., 2013). Accordingly, we firstly tested if the 3D models of plants obtained via SFM have the accuracy to be further classified into leaves and stem. This issue was satisfactorily addressed by successfully calibrating and validating a machine learning classification algorithm (RF), which used point-wise saliency features and color indices as predictor of leaves and stem.

The use of colors as suggested by Dey et al. (2012) as plant structure predictors was further extended using color indexes (GI, RI, BI) assigned to each xyz point rather than the raw RGB val-

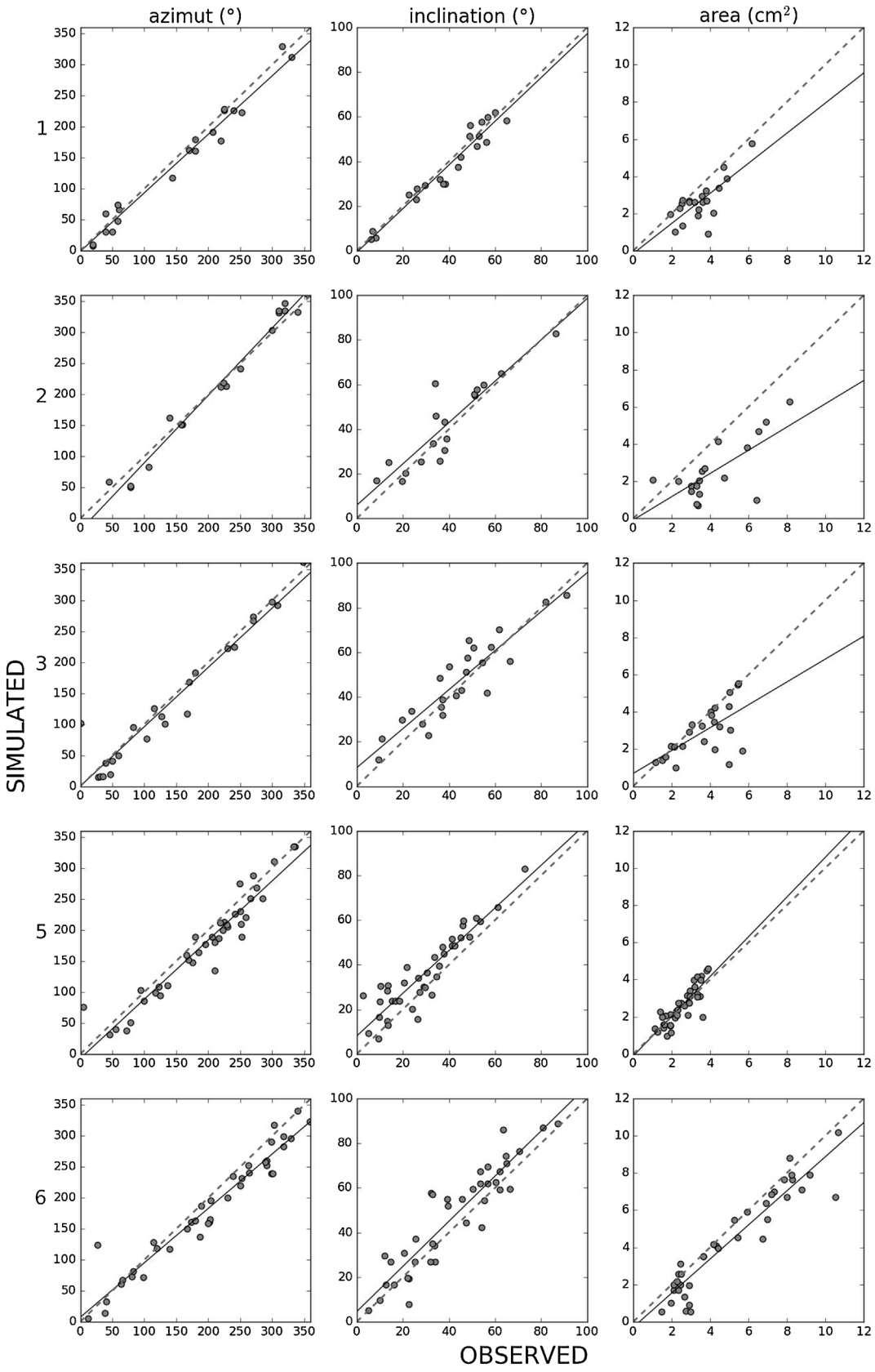

Fig. 6. Plot measured-estimated data for leaf azimuth, inclination and area on sub-sample leaves of 5 olive tree branches. The dotted lines represent 1:1 agreement. The regression analysis statistics for each plant are reported in Table 2.

Table 2
Statistical tests and goodness of fit for subsampled leaves and total leaf number on a branch; Legend: Az = Azimuth (°), In = inclination (°), Ar = area (cm^2). For the regression analysis: int = intercept, slp = slope and R = correlation coefficient of the regression line (*** significant for P < 0.01, ** significant for P < 0.05); » not performed since only a subsample of leaves was considered; # single unit comparison was not performed. Intercepts and slopes statistically different from 0 and 1 respectively, are in bold. Statistical significance was tested using ANOVA ($P \leq 0.05$). In Kolgromov-Smirnov test (KS) P values are provided where the homogeneity of distribution is accepted for P > 0.05.

Plant	Observed-simulated data Regression analysis									Error indices								
	Az			In			Ar			MAE			RMSE			KS test (P)		
	int	*slp*	*R*	*int*	*slp*	*R*	*int*	*slp*	*R*	Az	In	Ar	Az	In	Ar	Az	In	Ar
1	7.25	0.92	0.96***	1.16	0.96	0.94***	−0.15	0.80	0.75**	20.62	4.12	0.84	26.69	5.66	1.10		»	
2	−19.16	**1.08**	0.98***	6.75	0.90	0.91***	0.01	**0.61**	0.72**	15.1	6.42	1.73	17.45	8.57	2.06		»	
3	0.15	0.96	0.96***	**8.25**	0.87	0.91***	0.83	**0.56**	0.61**	18.40	6.80	0.87	27.66	8.35	1.44	0.84	0.32	<0.05
4	#															0.71	0.34	<0.05
5	−7.43	0.95	0.96***	**8.08**	0.95	0.91**	−0.08	1.06	0.85**	23.07	8.01	0.40	28.28	9.72	0.51		»	
6	7.20	**0.88**	0.96***	4.27	1.03	0.92**	−0.20	0.90	0.93***	23.63	8.36	0.77	30.93	10.58	1.11		»	

ues. RGB brightness levels are in fact prone to the influence of changes in scene illumination, both solar and image exposure that are instead suppressed using color indices (Migliavacca et al., 2011). Our experiment demonstrated that a single RF model, calibrated and validated on a single branch, may be successfully applied to other samples with pictures taken in different light conditions and phenological stages. This provided evidence of the effectiveness of the proposed training strategy and of its potential use as a semi-automatic classification procedure in phenotyping process.

In our experiment, colors played a major role as discriminants of plant structures and saliency features improved the accuracy of RF in predicting points belonging to leaves and stem. The scale at which saliency features were calculated (i.e. the KD-tree dimensions) determined the final classificatory performances.

The identification of the scale that maximizes the differences between linear (stem) and planar (leaves) structures was constrained by two main factors: the minimum number of points that allows a shape to be detected (too few points in the KD-tree reduces the effectiveness of saliency features in detecting differences between linear and planar surfaces) (Fig. 3a) and the maximum number of points that avoids the inclusion of points not strictly belonging to leaves or stem (Fig. 3d).

The good performances of this calibration strategy were supported by a pre-processing procedure that included a point cloud cleaning and sub sampling. The subsampling procedure united to the structure of the KD-tree was a fundamental step that, while it increased the computational efficiency by decreasing the points to be processed, allowed the capabilities of saliency features in shape recognition to be fully exploited. The point cloud resulting from the cleaning procedure presents dissimilarities in point density that actually depend on the quality of SFM reconstruction and cleaning procedure effects. The use of sub sampling reduced these dissimilarities, resulting in a point cloud with a fixed spatial resolution (0.6×0.6 mm) that improved the classification performances related to saliency features. In the specific case of an olive tree, where leaves are expanded along a major axis and their shape may be not dissimilar to that of a stem (Fig. 3a), the KD-tree was set up to retrieve a fixed number of points, rather than using a fixed range. When using a point cloud with a fixed scale, this resulted in a dynamic selection of areas to be included in the KD-tree for a stem (Fig. 7 that produced saliency features better discriminating lines (stem) and areas (leaves) with respect to a KD-tree with a fixed range (Fig. 7bc).

There are some limitations to using local geometry of plant organs for classification (Lalonde et al., 2006; Paulus et al., 2013) and filtering methods may be applied to correct points that, under some circumstances, may be misclassified (Lalonde et al., 2006). The proposed filtering procedure improved the classification performances of RF, which resulted in increased ROC and TSS that shifted from 0.84 and 0.64–0.89 and 0.77, respectively. The analysis of the response of reclassification performances indicated that the best results are obtained selecting a threshold >0.6 to convert a point initially classified as stem into a leaf (<0.6 to convert a point classified as leaf into stem). This asymmetry is likely related to the best performances of RF in the identification of the entire leaf surfaces, whereas the classification of a stem is more problematic due to a greater variability in dimensions, which in some cases may approximate those of a leaf, and color, which is green in the new growing wood. As a result, pointwise classification of a stem is noisier than that of a leaf and a high threshold to convert one class into another preserves the good result obtained for the leaves that are almost correctly classified, while it increases the range to detect a stem in a noisy region.

The results obtained on segmented leaves, on both sub-samples and the entire population, provided evidence that, using the proposed technique, SFM may be effectively applied for retrieving the basic features of plant architecture, in particular leaf inclination and azimuth, whereas the leaf area was generally underestimated.

The visual analysis of leaves sub-samples whose area was underestimated (especially in branches 1–3) indicated that this underestimation was due to a reduced capability of SFM to accurately reproduce, in some cases, the entire leaf area, which appeared truncated. In these cases, after removing the area of the leaves that were only partially reconstructed, the relationship between observed and simulated data significantly improved (data not shown). This indicates that when the system had correctly reconstructed the leaf blade, the leaf area was correctly estimated.

The analysis of leaf inclination, azimuth and area indicated that the proposed technique was able to detect the overall metrics of plant structures with uncertainties for leaf area estimation. The results of the KS test further highlighted that this system faithfully reproduced the distribution of leaf inclination and azimuth of an entire branch, confirming a significant under-estimation of leaf area. As observed in Fig. 6, this is likely related to an incomplete leaf reconstruction that may occur in the case of leaf mutual occlusion.

As a matter of fact, the proved capability of this framework to provide quantitative information of plant structure even in a complex canopy like that of olive tree, indicated that SFM approach may be suggested as a way to set up a low cost phenotyping platform. This, in its preliminary structure, would be basically cantered on the use of digital camera mounted on a belt conveyor that records digital images at a fixed time lapse (for details please visit https://www.youtube.com/watch?v=Wal3bi-ZS7o). This simple structure, when applied in a controlled environment, would result into a speed up in the measurement of plant architectural parameters that are time consuming or inaccurate when considering the complex structure of a canopy.

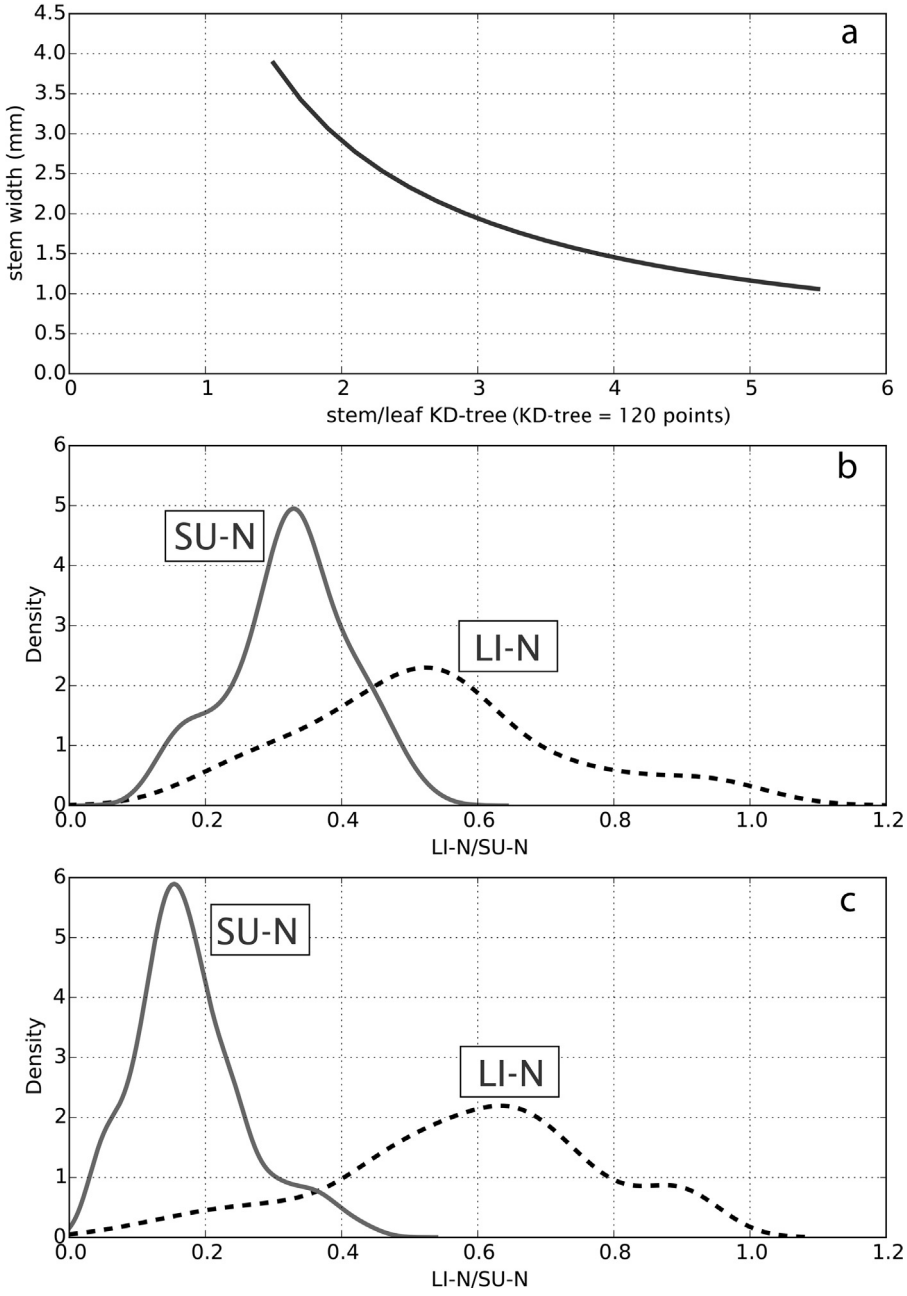

Fig. 7. (a) Ratio between the maximum dimensions obtained for a stem and a leaf for a KD–tree = 120 points spaced 0.6 × 0.6 mm. For the leaf, the maximum dimension of the KD-tree corresponded to the diameter of a circle having area A = 120 × 0.36 mm^2 (7.4 mm). For the stem, the maximum dimension was obtained considering a rectangle having area A and different widths; (b) Probability density function of linear-ness (LI-N, black line) and surface-ness (SU-N, grey line) calculated for a point cloud of a stem spaced 0.6 × 0.6 mm using a KD-tree populated with points from a fixed range (3.7 mm); (c) Probability density function of linear-ness (LI-N, black line) and surface-ness (SU-N, grey line) calculated for a point cloud of a stem spaced 0.6 × 0.6 mm using a KD-tree populated with the nearest 120 points. The results were compared with (b) considering that 120 points (the threshold optimizing classification performance) spaced 0.6 × 0.6 mm would correspond to a circle with a diameter of 7.4 mm.

5. Conclusions

This study evaluated the feasibility of the SFM approach for retrieving plant structural parameters. 3D point cloud models obtained using SFM, were pre-processed (cleaning and subsampling), classified (leaves and stem), post-processed (filtering) and segmented (identification of single leaves). The overall results pointed out that SFM included in this technique may provide more insight into the analysis of plant architecture in terms of a faithful description of leaf inclination azimuth whereas some improvements are needed for leaf area estimation. Nevertheless, some issues arose from our analysis and these may be briefly listed:

The capability of SFM to produce a point cloud is strictly related to the capacity of the camera to focus on the objects along its xyz axis. In other words, SFM may be difficult to apply on plant structures expanded in depth because particularly distant objects may be out of focus and this would result in a loss of points that can be detected and tracked for 3D reconstruction. In our case, we coupled reduced lens aperture with long exposure times that allowed depth of field to be maximized and to keep objects in the background in focus as much as possible.

Pictures were taken indoors under diffuse light conditions to reduce the influences of natural environment such as direct illumination, which decreases the visible texture of the plant, or

disturbance factors such as wind, which increases the uncertainty in the xyz positioning of a not fixed point. As such, given the complexity of the plant being analyzed and drawbacks related to the use of a digital camera with a long exposure time, further experiments are required to test if SFM may be effectively used in the open field, especially in the continuous and automated monitoring of the vegetation status of a woody species

The point clouds generated by SFM were in some cases particularly noisy and this required a cleaning procedure that, while improving a correct structure classification, likely resulted in a loss of information.

Manual editing still plays an important role for improving the classification and segmentation processes by using a cleaning procedure and manually separating/joining plant material partially or incorrectly reconstructed. Nevertheless, in some cases it was not possible to reconstruct entire leaf blades due to mutual occlusion and this resulted in a severe underestimation of single leaf area. Accordingly, further studies are needed to improve the performances of the approach.

Acknowledgments

The authors would like to gratefully acknowledge the constructive comments provided by anonymous referees. The authors would like to thank to Mr. Antonio Esposito of Department of Agri-Food Production and Environmental Sciences (DISPAA) and Dr. Barbara Stoltz of University of Marburg for technical assistance and Mr. Nicola Barbini for the useful hints he provided during several discussions.

References

Allouche, O., Tsoar, A., Kadmon, R., 2006. Assessing the accuracy of species distribution models: prevalence, kappa and the true skill statistic (TSS). J. Appl. Ecol. 43, 1223–1232, http://dx.doi.org/10.1111/j.1365-2664.2006.01214.x.

Brantley, S.T., Young, D.R., 2007. Leaf-area index and light attenuation in rapidly expanding shrub thickets. Ecology 88, 524–530.

Breiman, L., 2001. Random forest. Mach. Learn. 45, 5–32.

Chéné, D., Rousseau, P., Lucidarme, J., Bertheloot, V., Caffier, P., Morel, E., Belin, F., Chapeau-Blondeau, F., 2012. On the use of depth camera for 3D phenotyping of entire plants. Comput. Electron. Agric. 82, 122–127, http://dx.doi.org/10.1016/j.compag.2011.12.007.

Chianucci, F., Cutini, A., Corona, P., Puletti, N., 2014. Estimation of leaf area index in understory deciduous trees using digital photography. Agric. For. Meteorol. 198, 259–264, http://dx.doi.org/10.1016/j.agrformet.2014.09.001.

Confalonieri, R., Foi, M., Casa, R., Aquaro, S., Tona, E., Peterle, M., Boldini, A., De Carli, G., Ferrari, A., Finotto, G., Guarneri, T., Manzoni, V., Movedi, E., Nisoli, A., Paleari, L., Radici, I., Suardi, M., Veronesi, D., Bregaglio, S., Cappelli, G., Chiodini, M.E., Dominoni, P., Francone, C., Frasso, N., Stella, T., Acutis, M., 2013. Development of an app for estimating leaf area index using a smartphone. Trueness and precision determination and comparison with other indirect methods. Comput. Electron. Agric. 96, 67–74, http://dx.doi.org/10.1016/j.compag.2013.04.019.

Cutler, D.R., Edwards Jr, T.C., Beard, K.H., Cutler, A., Hess, K.T., Gibson, J., Lawler, J.J., 2007. Random Forests for classification in ecology. Ecology 88, 2783–2792, http://dx.doi.org/10.1890/07-0539.1.

Díaz-Varela, R.A., de la Rosa, R., León, L., Zarco-Tejada, P.J., 2015. High-resolution airborne UAV imagery to assess olive tree crown parameters using 3D photo reconstruction: application in breeding trials. Remote Sens. 7, 4213–4232, http://dx.doi.org/10.3390/rs70404213.

Dandois, J.P., Ellis, E.C., 2010. Remote sensing of vegetation structure using computer vision. Remote Sens. 2, 1157–1176, http://dx.doi.org/10.3390/rs2041157.

Dey, D., Mummert, L., Sukthankar, R., 2012. Classification of plant structures from uncalibrated image sequences, Applications of Computer Vision (WACV), 2012. In: IEEE Workshop on Applications and Computer Vision, IEEE, pp. 329–336.

Evans, J.S., Murphy, M.A., Holden, Z.A., Cushman, S.A., 2011. Modeling species distribution and change using random forest. In: Predictive Species and Habitat Modeling in Landscape Ecology. Springer, New York, pp. 139–159.

Fuentes, S., Palmer, A.R., Taylor, D., Zeppel, M., Whitley, R., Eamus, D., 2008. An automated procedure for estimating the leaf area index (LAI) of woodland ecosystems using digital imagery, MATLAB programming and its application to an examination of the relationship between remotely sensed and field measurements of LAI. Funct. Plant Biol. 35, 1070–1079, http://dx.doi.org/10.1071/FP08045.

Girardeau-Montaut, D., 2011. CloudCompare—Open Source project. OpenSource Project, http://www.danielgm.net/cc/> (accessed Aug. 5, 2015.).

Hanley, J.A., McNeil, B.J., 1982. The meaning and use of the area under a receiver operating characteristic (ROC) curve. Radiology 143, 29–36.

Ign, 2013. Micmac documentation. Retrieved July 24, 2014, from <http://logiciels.ign.fr/?Micmac>.

Ivanov, N., Boissard, P., Chapron, M., Andrieu, B., 1995. Computer stereo plotting for 3-D reconstruction of a maize canopy. Agric. For. Meteorol. 75, 85–102, http://dx.doi.org/10.1016/0168-1923(94)02204-W.

James, M.R., Robson, S., 2012. Straightforward reconstruction of 3D surfaces and topography with a camera: accuracy and geoscience application. J. Geophys. Res.: Earth Surf. 117, F03–017, http://dx.doi.org/10.1029/2011JF002289.

Jay, S., Rabatel, G., Hadoux, X., Moura, D., Gorretta, N., 2015. In-field crop row phenotyping from 3D modeling performed using Structure from Motion. Comput. Electron. Agric. 110, 70–77, http://dx.doi.org/10.1016/j.compag.2014.09.021.

Lalonde, J.F., Vandapel, N., Huber, D.F., Hebert, M., 2006. Natural terrain classification using three-dimensional ladar data for ground robot mobility. J. Field Robot. 23, 839–862.

Li, L., Zhang, Q., Huang, D., 2014. A review of imaging techniques for plant phenotyping. Sensors 14, 20078–20111, http://dx.doi.org/10.3390/s141120078.

Liu, J., Pattey, E., Admiral, S., 2013a. Assessment of in situ crop LAI measurement using unidirectional view digital photography. Agric. For. Meteorol. 169, 25–34, http://dx.doi.org/10.1016/j.agrformet.2012.10.009.

Liu, C., Kang, S., Li, F., Li, S., Du, T., 2013b. Canopy leaf area index for apple tree using hemispherical photography in arid region. Sci. Hortic. 164, 610–615, http://dx.doi.org/10.1016/j.scienta.2013.10.009.

Müller-Linow, M., Pinto-Espinosa, F., Scharr, H., Rascher, U., 2015. The leaf angle distribution of natural plant populations: assessing the canopy with a novel software tool. Plant Methods 11, 11, http://dx.doi.org/10.1186/s13007-015-0052-z.

Macfarlane, C., Hoffman, M., Eamus, D., Kerp, N., Higginson, S., McMurtrie, R., Adams, M., 2007. Estimation of leaf area index in eucalypt forest using digital photography. Agric. For. Meteorol. 143, 176–188, http://dx.doi.org/10.1016/j.agrformet.2006.10.013.

Mathews, A.J., Jensen, J.L., 2013. Visualizing and quantifying vineyard canopy LAI using an unmanned aerial vehicle (UAV) collected high density structure from motion point cloud. Remote Sens. 5, 2164–2183, http://dx.doi.org/10.3390/rs5052164.

Migliavacca, M., Galvagno, M., Cremonese, E., Rossini, M., Meroni, M., Sonnentag, O., Cogliati, S., Manca, G., Diotri, F., Busetto, L., Cescatti, A., Colombo, R., Fava, F., Morra di Cella, U., Pari, E., Siniscalco, C., Richardson, A.D., 2011. Using digital repeat photography and eddy covariance data to model grassland phenology and photosynthetic CO_2 uptake. Agric. For. Meteorol. 151, 1325–1337, http://dx.doi.org/10.1016/j.agrformet.2011.05.012.

Paulus, S., Dupuis, J., Mahlein, A.K., Kuhlmann, H., 2013. Surface feature based classification of plant organs from 3D laserscanned point clouds for plant phenotyping. BMC Bioinf. 14, 238 http://www.biomedcentral.com/1471-2105/14/238.

Phattaralerphong, J., Sinoquet, H., 2005. A method for 3D reconstruction of tree crown volume from photographs: assessment with 3D-digitized plants. Tree Physiol. 25, 1229–1242.

Phattaralerphong, J., Sathornkich, J., Sinoquet, H., 2006. A photographic gap fraction method for estimating leaf area of isolated trees: assessment with 3D digitized plants. Tree Physiol. 26, 1123–1136, http://dx.doi.org/10.1093/treephys/26.9.1123.

Pisek, J., Ryu, Y., Alikas, K., 2011. Estimating leaf inclination and G-function from leveled digital camera photography in broadleaf canopies. Trees 25, 919–924, http://dx.doi.org/10.1007/s00468-011-0566-6.

Pollefeys, M., Gool, L.V., Vergauwen, M., Verbiest, F., Cornelis, K., Tops, J., 2004. Visual modeling with a hand-held camera. Int. J. Comput. Vis. 59, 207–232.

Rose, J.C., Paulus, S., Kuhlmann, H., 2015. Accuracy analysis of a multi-view stereo approach for phenotyping of tomato plants at the organ level. Sensors 15, 9651–9665.

Ryu, Y., Sonnentag, O., Nilson, T., Vargas, R., Kobayashi, H., Wenk, R., Baldocchi, D.D., 2010. How to quantify tree leaf area index in a heterogeneous savanna ecosystem: a multi-instrument and multimodel approach. Agric. For. Meteorol. 150, 63–76, http://dx.doi.org/10.1016/j.agrformet.2009.08.007.

Santos, T.T., de Oliveira, A.A., 2012. Image-based 3D digitizing for plant architecture analysis and phenotyping. In: Workshop on Industry Applications (WGARI) in SIBGRAPI 2012 (XXV Conference on Graphics, Patterns and Images), Ouro Preto, MG, Brazil, pp. 21–28.

Snavely, N., Seitz, S.M., Szeliski, R., 2008. Modeling the world from internet photo collections. Int. J. Comput. Vis. 80, 189–210, http://dx.doi.org/10.1007/s11263-007-0107-3.

Turner, D., Lucieer, A., Watson, C., 2011. Development of an unmanned aerial vehicle (UAV) for hyper resolution mapping based visible, multispectral, and thermal imagery. In: Proceedings of 34th International Symposium of Remote Sensing Environment, Sydney, NSW, Australia, pp. 10–15 (April 2011).

Weiss, U., Biber, P., 2011. Plant detection and mapping for agricultural robots using a 3D LIDAR sensor. Robot. Auton. Syst. 59, 265–273, http://dx.doi.org/10.1016/j.robot.2011.02.011.

Wu C., 2011. VisualSFM: A Visual Structure from Motion System. http://homes.cs.washington.edu/?ccwu/vsfm/2011.

Yang, Y., Zhang, D., 2003. A novel line scan clustering algorithm for identifying connected components in digital images. Image Vision Comput. 21, 459–472, http://dx.doi.org/10.1016/S0262-8856(03)00015-5.
Yihang, F., Chengda, L., Ruifang, Z., Yao, T., Xingyu, W.A., 2014. New Approach for Measuring 3D Digitalized Rape Leaf Parameters based on Images. In: Third International Conference on Agro-Geoinformatics (Agro-Geoinformatics 2014), Beijing, China 11–14 August 2014, ISBN: 978-1-4799-4156-8.
Zarco-Tejada, P.J., Diaz-Varela, R., Angileri, V., Loudjani, P., 2014. Tree height quantification using very high resolution imagery acquired from an unmanned aerial vehicle (UAV) and automatic 3D photo-reconstruction methods. Eur. J. Agron. 55, 89–99, http://dx.doi.org/10.1016/j.eja.2014.01.004.
Zou, X., Mõttus, M., Tammeorg, P., Torres, C.L., Takala, T., Pisek, J., Mäkelä, P., Stoddard, F.L., Pellikka, P., 2014. Photographic measurement of leaf angles in field crops. Agric For. Meteorol. 184, 137–146, http://dx.doi.org/10.1016/j.agrformet.2013.09.010.